J Low Temp Phys (2008) 151: 125–130
DOI 10.1007/s10909-007-9627-z

Energy Collection Efficiency of Tungsten Transition-Edge Sensors in the Near-Infrared

A.E. Lita · A.J. Miller · S. Nam

Received: 22 July 2007 / Accepted: 15 September 2007 / Published online: 9 January 2008

Abstract Single-photon detectors operating at visible and near-infrared wavelengths with high detection efficiency and low noise are a requirement for many quantum-information applications. Detection of visible and near-infrared light at the single-photon level and discrimination between one- and two-photon absorption events place stringent requirements on TES design in terms of heat capacity, thermometry, and optical detection efficiency. Energy loss in the conversion of the photon energy in tungsten TESs to heat degrades the performance of these devices. By fabricating TESs on surface-micromachined Si_3N_4 membranes we improved the energy collection efficiency by a factor of two, to ∼80% energy efficiency.

Keywords Single-photon detector · Electron-phonon thermal coupling

PACS 74.25.Kc · 85.25.Pb · 85.25.Oj

1 Introduction

Superconducting transition-edge sensors (TESs) are microcalorimeters that can be optimized for particular wavelengths from X-ray to near-infrared, based on the material choice and size of different components [1]. A microcalorimeter consists of an absorber for the incident photons, a thermometer to measure the resulting temperature increase and a weak thermal link enabling the return to base temperature after measurement. TESs for visible and near-infrared wavelengths have been fabricated

A.E. Lita (✉) · S. Nam
Optoelectronics Division, NIST, Boulder, CO, USA
e-mail: lita@boulder.nist.gov

A.J. Miller
Physics Department, Albion College, Albion, MI, USA

from tungsten (W) due to the tunability of its superconducting transition temperature (T_c) in the ∼100 mK range and the relative weak coupling between its electron and phonon systems at these temperatures [2]. Detection of visible and near-infrared light at the single-photon levels places stringent requirements on the heat capacity and thermometry. For the W TESs, the electron subsystem in a thin film of W is both the absorber and the thermometer. The anomalously low thermal coupling between the electrons and phonons in W provides the weak thermal link.

Tungsten TESs have been shown to display an energy resolution of ∼0.15 eV FWHM for single infrared, optical and ultraviolet photons (350 nm–4 μm) [2]. However, the excellent energy resolution of the W TESs is degraded by the collection efficiency. During the photon thermalization process, high-energy phonons are no longer confined to the W electron system and can escape into the substrate unmeasured, consequently degrading the energy resolution of the sensor. Previous work [2] has shown that a fraction 0.42 of the total photon energy is deposited in the W electron system following the photoelectron cascade. In this paper we present our results on fabrication of W TESs on Si_3N_4 membranes in order to provide a way to recover the high-energy phonons produced at the absorption of a photon.

2 Device Fabrication

Thermal isolation for cryogenic thermal detectors is often provided by low-stress Si_3N_4 membranes formed by bulk or surface micromachining. A review of micromachining techniques used by other groups for creation of various thermal-isolation structures can be found in [1]. In this work we used a similar surface micromachining technique [3] that uses XeF_2 gas phase chemical etch [4] to create Si_3N_4 membranes on Si wafers. Generally, micromachined membranes can display fairly complicated geometries including very thin membranes legs and spider-web [1] structures in order to minimize system thermal conductance. Because we operate in the electron-phonon-limited heat conduction [2], minimizing the phonon-phonon coupling between the sensor and substrate has no effect on our device thermal system, and our membrane's geometry is very simple.

A challenging aspect of W TES fabrication is control of the superconducting critical temperature, T_c. Sputtered thin films of W consist of a combination of two crystallographic phases, α and β, with different T_cs. The ratio of the two crystallographic phases, and consequently the film T_c can be tuned by adjusting the deposition conditions [5].

The TESs were fabricated on Si wafers coated with 500 nm low stress Si_3N_4 (grown by a low-pressure chemical vapor deposition (LPCVD) technique). By opening lithographic windows in the Si_3N_4 layer we can isotropically etch the Si wafer using XeF_2 gas-phase chemical etch, forming membranes underneath our devices, as in Fig. 1. The W film, 20 nm thick, was deposited by DC sputtering in an UHV system, with a 5 nm amorphous Si *in situ* underlayer for T_c stabilization [5]. The W was then patterned into 25 × 25 μm squares by a ferricyanide-based wet etch. The wiring layer consisted of a ∼60 nm Al layer deposited by electron beam evaporation and patterned by a lift-off process. After completion of the TES fabrication, a window was opened into the Si_3N_4 layer next to the devices by a fluorine based reactive

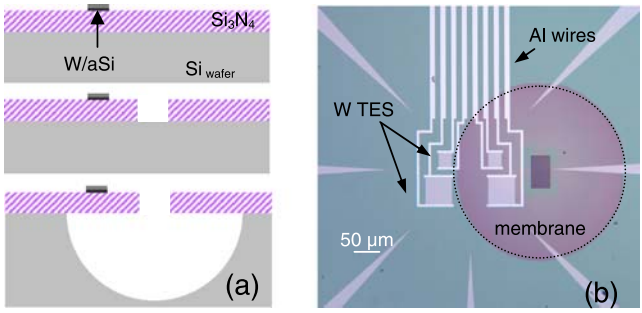

Fig. 1 (Color online) (**a**) Fabrication schematic for surface micromachining (not to scale). XeF_2 etches Si isotropically. (**b**) Optical image of four W TES with Al wiring next to a window etched in Si_3N_4. Two devices are on the Si_3N_4 membrane (outlined by a *dotted circle*) and two are still on the Si wafer

ion etch (RIE), Fig. 1(a). Using the same photoresist mask, the subsequent Si etch membrane definition step was accomplished in a pulse-type XeF_2 reactor [3]. In order to minimize device heating and etch rate, since the XeF_2-Si reaction is extremely exothermic, a 1:1 mixture of XeF_2 and He was used. After membrane etching, the photoresist mask was removed in O_2 plasma.

A picture of the final device on a membrane is shown in Fig. 1(b). From profilometry measurements on similar etched structures, the W TES device was ∼150 μm away from the etched Si wafer. Our fabrication allows us to compare device performance between a TES on a membrane vs. a TES directly on the Si wafer.

3 Device Testing

Measurements of the energy collection efficiency require coupling of light to the detectors. A 9 μm core single-mode telecommunication fiber was aligned at room temperature by backside through-chip alignment. Once the fiber was aligned, the detector was cooled to ∼55 mK in an adiabatic demagnetization refrigerator. Our optical setup, Fig. 2(a), included a pulsed 1550 nm laser source coupled to an attenuator in order to achieve low power levels at the detector.

The detector electron system temperature was maintained within its superconducting to normal transition ($T_c \sim 100$ mK) via Joule heating produced by a voltage bias. The stability of the voltage bias is due to negative electro-thermal feedback (ETF) [6], where an increase in sensor temperature and correspondent increase in sensor resistance decreases the Joule heating ($\sim V^2/R$). When a photon is absorbed, it produces a photoelectron that heats up the W electron system. This heat in excess of the quiescent Joule heating at equilibrium is removed through negative ETF in the form of a drop in the Joule power dissipation. Consequently, the energy absorbed in the W electron system can be calculated by multiplication of the integral of change in current with the bias voltage, $E = V_{bias} \int \Delta I(t) dt$.

Figure 2(b) depicts our measurement setup including the voltage bias electrical circuit. Voltage biasing is achieved by use of a stable room-temperature current source

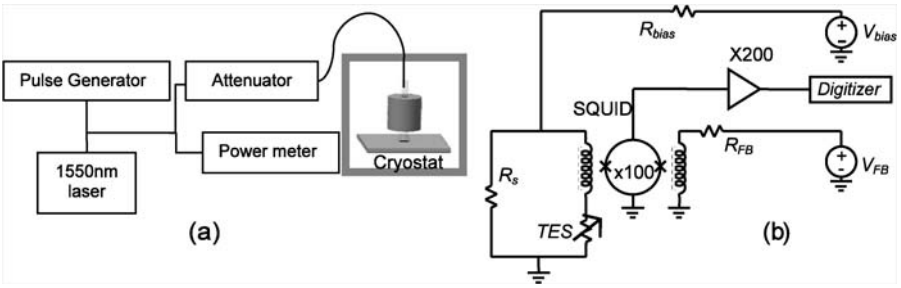

Fig. 2 (**a**) Optical diagram depicting coupling of an attenuated pulsed 1550 nm source to the TES in the cryostat. (**b**) Schematic of the electrical circuit

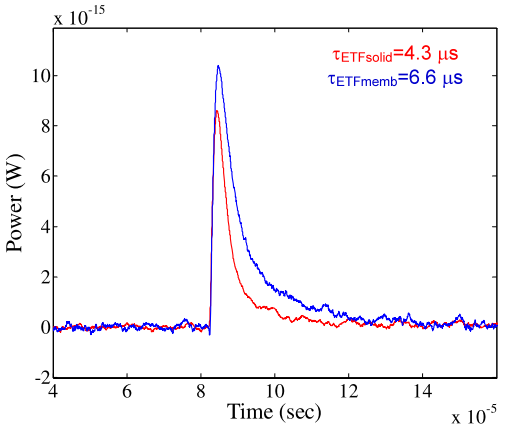

Fig. 3 (Color online) Change in power dissipation of single-photon pulses for membrane device (*blue*), higher signal, and for solid device (*red*)

followed by a 20 mΩ cold (4 K) shunt resistor (R_s) in parallel with the TES. A low-noise cryogenic preamp consisting of an array (100) of dc superconducting quantum interference devices (SQUID) amplifies the sensor current. The sensor current induces a flux through the SQUID via the input coil. The amplified signal is then recorded on an oscilloscope/digitizer and the sensor current change can subsequently be extracted by using the measured transimpedance gain of the amplifier chain.

Figure 3 displays detector response to 1550 nm (0.8 eV) single photons, for detector on membrane and Si wafer, respectively. The decay time is 6.6 μs for the membrane device and 4.3 μs for the solid device. By integration of the area under the pulses we obtained energy efficiency of 83% for the device on the Si_3N_4 membrane and 47% for device on the Si wafer. Hence, by placing the detector on the membrane we increased energy collection efficiency by almost a factor of two. Using these measured efficiency factors we can predict the resolution for both devices, on the membrane and on Si. We used the W electronic heat capacity, given by $C = \gamma T$ with $\gamma = 1.3$ mJ/(mole-K^2), multiplied by the 2.43 factor from the Bardeen-Cooper-Schrieffer (BCS), corresponding to the increase in heat capacity of a superconductor just below T_c. We obtained 0.44 fJ/K for the membrane device and 0.52 fJ/K for the solid device, for a detector volume of 25 μm × 25 μm × 20 nm. The measured T_cs are 106 ± 5 mK for the membrane device and 128 ± 6 mK for the solid device. The

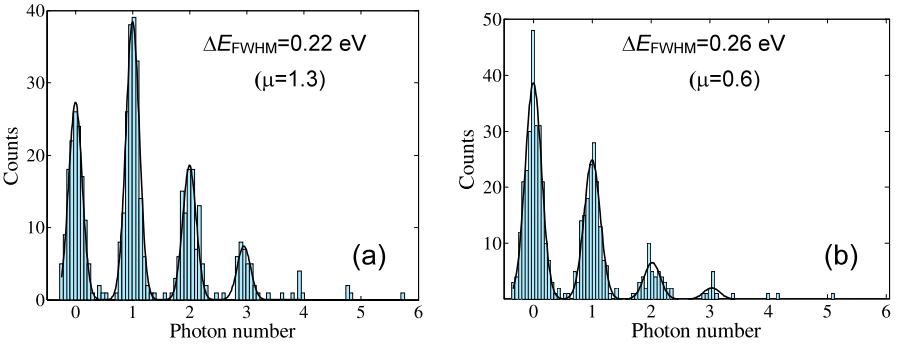

Fig. 4 (Color online) Histograms of pulse heights at illumination with a pulsed 1550 nm source with mean photon number μ. (**a**) Membrane device, (**b**) solid device. The acquisition of data was triggered by the laser trigger. The *black line* represents a fit of Gaussian functions to the data

difference in T_c values may be due to membrane device processing. From the I–V curves of our devices we extracted the power in the self-biased region, known as the quiescent power, as $P_0 = 350$ fW for the membrane device and $P_0 = 260$ fW for the solid device. For substrate temperatures well below T_c we can estimate the thermal conductances using the formula $g = dP/dT \sim nP_0/T_c$. We obtained 16 pW/K and 10 pW/K as the thermal conductances for membrane and solid devices, respectively.

Consequently, the intrinsic time constants $\tau_0 = C/g$, are 27 μs and 51 μs for the membrane and solid devices, respectively. The actual time constants that we measured are shorter due to ETF and relate to the intrinsic time constants through $\tau_{\mathrm{ETF}} = \tau_0/(1 + \alpha/n)$, where $\alpha = (d \ln R/d \ln T)_{V=constant}$, and describes the sharpness of the superconducting transition [6]. We estimate α as 15 and 54 for the membrane and solid device, respectively. The theoretical energy resolution [6] limit is given by $\Delta E_{\mathrm{FWHM}} = 2.355\sqrt{4k_B T_c^2 C(1/\alpha)\sqrt{(n/2)}}$. Using the estimated values of $\alpha, C, n = 5$ (for electron-phonon limited conductance [2]), and measured T_cs we can calculate the expected energy resolutions. With the efficiency factors measured as 83% for the membrane device and 47% for the solid device, the predicted resolution is 0.095 eV and 0.12 eV for the membrane and solid devices, respectively.

Our measured values from the histograms of pulse heights, Fig. 4, for the full width half maximum (FWHM) for the membrane and solid devices are 0.22 eV and 0.26 eV, respectively. Both devices give excellent discrimination between one- and two-photon events. However, by placing the detector on a membrane we increased the energy resolution. Since this improvement in energy resolution is directly related to significant energy collection improvement, full collection of photons energy could eliminate any phonon-loss noise mechanism such as downconversion phonon noise [7].

The measured energy resolution values for both membrane and solid devices are consistently larger than the values obtained from calculations. The measured noise for each of the devices at the operating points is 9 pA/$\sqrt{\mathrm{Hz}}$ and 11 pA/$\sqrt{\mathrm{Hz}}$, values comparable to the expected current noise of the SQUID amplifiers, indicating that significant improvement to resolution maybe possible with lower noise SQUIDs.

4 Conclusions

By fabricating the W TESs on a Si_3N_4 membrane we demonstrated a significant improvement in the fraction of energy collection from 47% to 83%. We also measured better energy resolution for the detectors fabricated on membranes. Optimization of device operation on membranes could lead to significant improvement in device resolution.

References

1. K.D. Irwin, G.C. Hilton, *Cryogenic Particle Detection*. Topics Appl. Phys., vol. 99 (Springer, Berlin, 2005), pp. 63–149
2. B. Cabrera, R.M. Clarke, P. Colling, A.J. Miller, S. Nam, R.W. Romani, Appl. Phys. Lett. **73**, 735 (1998)
3. G.C. Hilton et al., IEEE Trans. Appl. Supercond. **13**, 664 (2003)
4. F.I. Chang et al., Proc. SPIE **2641**, 117 (1995)
5. A.E. Lita et al., IEEE Trans. Appl. Supercond. **15**, 3528 (2005)
6. K.D. Irwin, Appl. Phys. Lett. **66**, 1998 (1995)
7. A.G. Kozorezov, J.K. Wigmore, D. Martin, P. Verhoeve, A. Peacock, Appl. Phys. Lett. **89**, 223510 (2006)